Classical chaotic scattering-periodic orbits, symmetries, multifractal invariant sets

1990 J. Phys. A: Math. Gen. 23 2847

(http://iopscience.iop.org/0305-4470/23/13/023)

J. Phys. A: Math. Gen. **23** (1990) 2847–2866. Printed in the UK

Classical chaotic scattering—periodic orbits, symmetries, multifractal invariant sets

Christof Jung and Peter H Richter

Fachbereich Physik und Institut für Dynamische Systeme, Universität Bremen, D-2800 Bremen 33, Federal Republic of Germany

Received 9 November 1989

Abstract. The infinite set of periodic orbits of a chaotic system is investigated. Their globally exact symbolic dynamics is related to Birkhoff's method of iterated symmetry lines which produces symmetric periodic orbits of various classes. A complete picture emerges as to what part of the periodic orbits can be obtained by means of the Birkhoff lines. In addition, the thermodynamic formalism is applied to the multifractal structure created by the horseshoe arrangement of the periodic orbits.

1. Introduction

Chaos in a classical dynamical system derives from the existence of homoclinic or heteroclinic intersections of the invariant manifolds of unstable periodic orbits. The scaling properties of their fractal structures are intimately related to the eigenvalues of those periodic orbits. (We shall speak of eigenvalues of periodic orbits when we mean the eigenvalues of the Jacobian matrix at the corresponding periodic orbit in some Poincaré section.) An analysis of a chaotic system thus requires the knowledge of its most important periodic orbits. No systematic methods exists that generates *all* periodic orbits in an arbitrary system. For Hamiltonian systems, however, the method of symmetry lines has been developed into a powerful tool to produce a subset of the periodic orbits, namely those which possess certain symmetries [1]. The essence of the method is to iterate a few lines related to time reversal symmetry, in the Poincaré surface of section, and obtain the periodic orbits as intersections of those iterated lines. It is well known that this method does not, in general, yield all periodic orbits.

Therefore it is instructive to investigate a chaotic system where a complete survey on all periodic orbits can be obtained by other methods. By comparison we will see which subset of the periodic orbits derives from symmetry properties.

A classical potential scattering system where this is indeed possible has been known for some time [2, 3]. The potential in a two-dimensional configuration space with Cartesian coordinates x, y is

$$V(x,y) = \exp[-y^2 - (x+\sqrt{2})^2] + \exp[-(y-\sqrt{3/2})^2 - (x-\sqrt{1/2})^2] + \exp[-(y+\sqrt{3/2})^2 - (x-\sqrt{1/2})^2]. \tag{1}$$

It was demonstrated in [2, 3] that there is chaos in the phase space of this triple hill potential, and how this manifests itself in the deflection function and in the scattering

0305-4470/90/132847+20$03.50

cross section. The interesting range of energies is between the saddle energy $E_s \approx 0.45$ and the energy of the hilltops, $E_m \approx 1.005$. In this range, almost all trajectories are scattering orbits, going to infinity for times $t \to +\infty$ or $t \to -\infty$. However, a non-trivial subset of the energy surface (of measure zero) consists of trajectories which are held between the three potential hills for all times, in past and future. Such trajectories will be called *localised* in the following. They are all unstable and form a hyperbolic invariant set.

Of particular importance for the present paper is the observation that there exists a binary symbolic dynamics to represent all localised orbits of the system in closed form. In section 2 we shall describe the symbolic dynamics again, and relate it to the potential's symmetry properties. In this connection we will introduce a symmetry reduced Poincaré mapping.

As usual in chaotic scattering systems, the most conspicuous periodic orbit oscillates back and forth on the potential's saddle. In section 3 we consider the invariant manifolds W^s and W^u of this orbit. For sufficiently high energies, $E > E_B \approx 0.485\ldots$, we find Smale's *horseshoe* in pure form, and on the closure of the lattice of intersections of W^s and W^u recover the binary symbolic dynamics. All localised orbits (and thus by necessity all periodic orbits) will be labelled by their corresponding 0/1 sequences. In section 4 we define symmetry lines in the Poincaré surface and their iterates. From their intersections we obtain subsets of the set of periodic orbits. The periodic orbits are grouped into symmetry classes, and a connection to symmetries of the symbol sequences is established.

The closure of the set of homoclinic and heteroclinic points of system (1) is a fractal set whose scaling and metric properties are approximately given by the eigenvalues of the two fixed points of the Poincaré map. These eigenvalues are energy dependent. In section 5 we analyse some of these properties in terms of their multifractal thermodynamics, i.e. we compute the potential $F(\beta)$ and, equivalently, the D_q respectively $f(\alpha)$ spectra.

2. Symmetry in configuration space and orbits

The potential of (1) has seven critical points. One is the minimum at $P_0 = (0,0)$, with energy $E_0 = 0.40\ldots$. There are three saddle points P_{s1}, P_{s2}, P_{s3} with energy $E_s = 0.45\ldots$; $P_{s1} = (0.6\ldots, 0)$, and the other two saddles are obtained by $\pm 2\pi/3$ rotation of P_{s1} about the centre. At energy $E_m = 1.005\ldots$ there are three maxima P_{m1}, P_{m2}, P_{m3}; $P_{m1} = (-1.4\ldots, 0)$, and the other two are again obtained by $\pm 2\pi/3$ rotation. The potential has C_{3v} symmetry. It vanishes sufficiently quickly for typical scattering trajectories to converge towards straight asymptotes for $t \to \pm\infty$. For $E < E_0$ and $E > E_m$ the system possesses no localised orbits and shows no signs of chaos. For $E \in (E_0, E_s)$ the energy surface has two disjoint components. Orbits in a neighbourhood of the origin are bounded; they fill a subset of phase space of positive measure. There are also scattering trajectories in this energy range. For $E \in (E_s, E_m)$ the localised orbits have measure zero in phase space. Chaos exists in the energy range $E \in (E_0, E_m)$.

In the following we shall restrict the discussion to the energy range $E \in (E_s, E_m)$. It was shown in [2] that there is topological chaos, and how it influences the scattering dynamics. In [3] the effects of this chaos on the scattering cross section was analysed. Figure 1 shows the equipotential lines for $E = 0.6$ together with three symmetry lines

$\sigma_1, \sigma_2, \sigma_3$, and two pieces of orbits. It will be useful later on to define the σ_i as half lines rather than full lines; so they start at P_0 and extend straight to infinity. V is invariant under reflections at σ_i. The set of three σ_i lines is itself invariant under C_{3v} operations.

For energies not too close to E_s, namely for $E > E_B \approx 0.485\ldots$, it has been verified that localised orbits do not enter a neighbourhood of the origin. For any localised orbit, and thus in particular for any periodic orbit, the sequence of crossings of the σ_i lines can be followed. Divide the trajectory into pieces as given by subsequent σ_i crossings. Let $d_j = k (k = 1, 2, \text{or } 3)$ if the jth crossing occurs at line σ_k. For each trajectory, this allows the construction of a 0/1 sequence $\{a_j, j \in \mathbb{Z}\}$, according to the scheme

$$a_j = 0 \qquad \text{if } d_{j+1} = d_j \tag{2}$$

$$a_j = 1 \qquad \text{if } d_{j+1} \neq d_j. \tag{3}$$

It is intuitively obvious that a binary sequence is adequate; consider figure 1. Let an orbit cross line σ_1 with positive $\dot{y}$. The next possible crossing is either with line σ_1 again, as in the right piece, or with line σ_2, as in the left piece. Thus after each crossing there is but a binary choice: to return to the line of the last crossing or to go on to the next. This simple observation is the basis for the binary signature that is defined in the following.

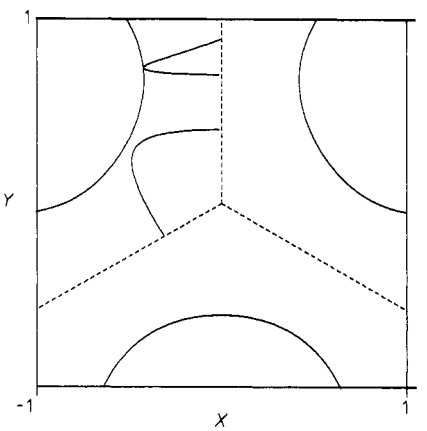

Figure 1. The energy boundary for $E = 0.6$ (three full line segments starting and ending at the frame boundary), the symmetry lines $\sigma_1, \sigma_2, \sigma_3$ (three broken half lines emanating from the origin), and two pieces of orbits in position space. The right piece is of $\frac{1}{2}\gamma$ type; it returns to the σ line from which it started. The other piece is of $\frac{1}{3}\Gamma$ type; it connects two different σ lines.

Two periodic orbits are particularly simple. First, let γ be the orbit corresponding to $a_j = 0 \forall j \in \mathbb{Z}$. This orbit oscillates back and forth across one of the three saddles. There are of course three such orbits, but as they are related by C_{3v} symmetry we shall identify them as *one* orbit γ. Second, let Γ be the orbit corresponding to $a_j = 1 \forall j \in \mathbb{Z}$. This orbit rotates around the origin in one of two possible orientations. (For illustrations of orbits γ and Γ see section 4.) The two orbits with different orientation are related by reflections at σ_i. They will thus be identified as *one* orbit Γ.

Other localised orbits can be described as follows. Each $a_j = 0$ in the sequence corresponds to a piece of orbit which resembles $\frac{1}{2}\gamma$, and each $a_j = 1$ corresponds to a piece which resembles $\frac{1}{3}\Gamma$. In this sense all localised orbits can be thought of as being composed from pieces similar to $\frac{1}{2}\gamma$ and to $\frac{1}{3}\Gamma$. (An analogous decomposition for the middle pieces of scattering orbits was given in [2].)

In order to investigate the binary symbolic dynamics in more detail, we need a Poincaré mapping. The following choice has turned out to be convenient; it incorporates the system's C_{3v} symmetry. Let the energy be fixed at a value E. For each crossing of a trajectory with any of the lines σ_1, σ_2, or σ_3 we record the distance r from the origin and the radial component p_r of the momentum (i.e. its projection on σ_i). Both orientations of crossings are taken because the σ_i are half lines. The surface of section $\mathcal{P}$ so defined is invariant under C_{3v} operations. A given point $\boldsymbol{x} \in \mathcal{P}$ thus represents six different phase space points which shall henceforth be identified.

Each localised orbit generates an infinite sequence of intersection points with the r/p_r plane. Generic scattering orbits, on the other hand, produce finite sets of points. In the energy range $E \in (E_s, E_m)$, almost all initial points in $\mathcal{P}$ correspond to scattering orbits with incoming and outgoing asymptotes; they have a first and a last intersection with the lines σ_i. The set Λ_+ of points in $\mathcal{P}$ which possess infinitely many images under the Poincaré map $P : \mathcal{P} \to \mathcal{P}$, has measure zero. Likewise, the set Λ_- of points with infinitely many pre-images has also zero measure. The localised orbits correspond to the set $\Lambda = \Lambda_+ \cap \Lambda_-$. In particular, Λ contains all periodic points of the map Poincaré map P.

Qualitatively similar behaviour has been discussed for a linear array of scatterers [4], for scattering off three hard discs [5, 6], and for a charged particle in the field of a magnetic dipole [7].

3. Symbolic dynamics in the Poincaré map

Chaotic scattering is closely related to the existence of unstable orbits which oscillate on top of a saddle point of the potential. Consider therefore the orbit γ and its corresponding point P_γ in the symmetry reduced Poincaré surface of section. Figure 2 depicts P_γ together with pieces of its stable manifold W^s and its unstable manifold W^u, for a typical energy in the range $E \in (E_B, E_m)$, where $E_B \approx 0.485$. (In [2] these manifolds were shown without symmetry reduction.) Because of time reversal invariance and the symmetry properties of σ_i, W^s and W^u are related via reflection at the r axis. Denoting time reversal by means of an overbar, we have $W^s = \overline{W^u}$, and it suffices to follow the course of W^u.

The branch X of W^u extends directly into the asymptotic range $r \to \infty$. The inner branch A of W^u leaves P_γ towards the point a_- at $r = 0$ from where it jumps to point a_+ because the intersection of the corresponding orbit is now with a different σ_i line, and the projection of the momentum is therefore different. The next piece B continues towards larger r-values and passes near P_γ before it returns to $r = 0$ at point b_-. From there W^u leaves figure 2 and re-enters later at point c_+. The last two pieces shown are C and D; the corresponding pieces of W^s are $\overline{A}$ through $\overline{D}$.

All subsequent pieces of W^u lie between $A \cup X$ and B, and all subsequent pieces of W^s lie between $\overline{A} \cup \overline{X}$ and $\overline{B}$. The homoclinic intersections of W^u and W^s are thus confined to the shaded area. It contains the closure Λ of the set of homoclinic points which is an invariant set with binary symbolic dynamics. So let us look in detail at

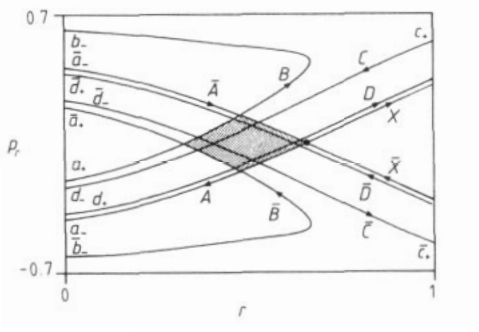

Figure 2. Some branches of the invariant manifolds of the fixed point P_γ (marked by a full circle) in the r/p_r plane, for $E = 0.6$. All localised orbits of the Poincaré map P are located within the hatched area.

the Poincaré map on this part of the r/p_r plane, see figure 3. It is a perfect example of Smale's horseshoe map.

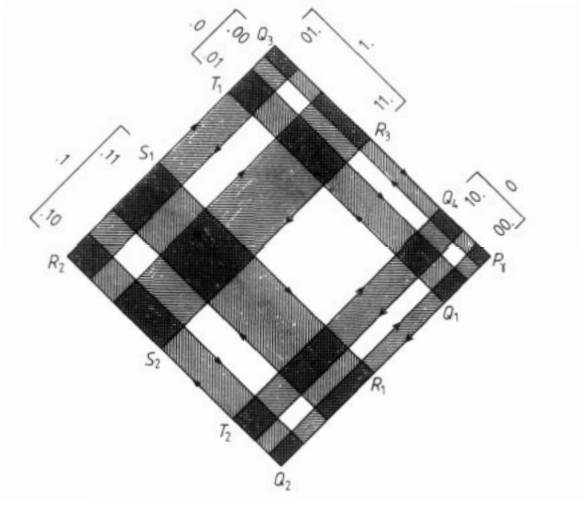

Figure 3. Schematic plot of the horseshoe dynamics in the hatched area of figure 2.

The nature of the map becomes clear if we consider special points on the invariant manifolds. Under the mapping P we have

$$Q_1 \mapsto Q_2 \mapsto Q_3 \mapsto Q_4$$
$$R_1 \mapsto R_2 \mapsto R_3$$
$$S_1 \mapsto S_2$$
$$T_1 \mapsto T_2.$$

The orbit in configuration space corresponding to the initial point S_1 was shown in figure 7(b) of [2]. If we define the four rectangles

$$\begin{aligned} .0 &:= P_\gamma Q_1 T_1 Q_3 \\ 0. &:= P_\gamma Q_2 T_2 Q_4 \\ .1 &:= R_1 Q_2 R_2 S_1 \\ 1. &:= R_2 Q_3 R_3 S_2 \end{aligned} \tag{4}$$

we have the mapping

$$\begin{aligned} &P : .0 \cup .1 \to 0. \cup 1. \\ &.0 \mapsto 0. \\ &.1 \mapsto 1.. \end{aligned} \tag{5}$$

In order to construct the sets $\Lambda_+, \Lambda_-, \Lambda$ recursively, we introduce the notation

$$\Lambda_+^1 := \{.0, .1\} \qquad \Lambda_-^1 := \{0., 1.\} \tag{6}$$

for the two sets of rectangles, and

$$\Lambda^1 := \{a_{-1}.a_1 = a_{-1}. \cap .a_1 | a_j \in \{0,1\}\} \tag{7}$$

for the set of their four intersections $0.0, 0.1, 1.0, 1.1$, with $\Lambda^1 = \Lambda_+^1 \cap \Lambda_-^1$. On Λ^1, both P and its inverse are defined. Thus we can identify the images and pre-images of its four parts:

$$\begin{aligned} \Lambda_+^2 &:= \{.a_1a_2 = P^{-1}(a_1.a_2) | a_j \in \{0,1\}\} \\ \Lambda_-^2 &:= \{a_{-2}a_{-1}. = P(a_{-2}.a_{-1}) | a_j \in \{0,1\}\}. \end{aligned} \tag{8}$$

All these strips are bounded by pieces of the invariant manifolds. The set of their intersections consists of sixteen parts and will be called Λ^2:

$$\Lambda^2 := \{a_{-2}a_{-1}.a_1a_2 = a_{-2}a_{-1}. \cap .a_1a_2 | a_j \in \{0,1\}\}. \tag{9}$$

Again we have $\Lambda^2 = \Lambda_+^2 \cap \Lambda_-^2$. Iterating this procedure we obtain a nested sequence of sets $\Lambda^n = \Lambda_+^n \cap \Lambda_-^n$

$$\Lambda^1 \supset \Lambda^2 \supset \ldots \supset \Lambda^n \supset \ldots$$

each consisting of 2^{2n} elements, with

$$\Lambda = \bigcap_{n=1}^{\infty} \Lambda^n. \tag{10}$$

By construction, Λ is invariant under P and P^{-1}. The operation of P is a right shift on Λ, P^{-1} operates as a left shift:

$$\begin{aligned} &P : \ldots a_{-n} \ldots a_{-2}a_{-1}.a_1a_2 \ldots a_n \ldots \mapsto \ldots a_{-n} \ldots a_{-2}a_{-1}a_1.a_2 \ldots a_n \ldots \\ &P^{-1} : \ldots a_{-n} \ldots a_{-2}a_{-1}.a_1a_2 \ldots a_n \ldots \mapsto \ldots a_{-n} \ldots a_{-2}.a_{-1}a_1a_2 \ldots a_n \ldots. \end{aligned} \tag{11}$$

The point P_γ is given by the symbol sequence $a_j = 0 \forall j \in \mathbb{Z} \setminus \{0\}$. There is another point with period 1, namely P_Γ, given by $a_j = 1 \forall j \in \mathbb{Z} \setminus \{0\}$. This point corresponds to the ring orbit Γ. Periodic sequences of a_j correspond to periodic orbits. The 0/1-sequences introduced here correspond precisely to the 0/1-sequences of section 2. The symbolic horseshoe dynamics thus reflects how orbits are composed of pieces similar to $\frac{1}{2}\gamma$ and $\frac{1}{3}\Gamma$. Points from Λ, i.e. two-sided infinite 0/1-sequences, correspond to localised orbits. Points from $\Lambda_+ \subset W^s$, i.e. from the infinite set of strips described

by the one-sided sequences $.a_1a_2a_3\ldots$, correspond to incoming scattering orbits that never leave the potential. Points from $\Lambda_- \subset W^u$, i.e. from the set of strips described by the one-sided sequences $\ldots a_{-3}a_{-2}a_{-1}.$, correspond to outgoing scattering orbits that never came in.

In summary, the dynamics on an energy surface with E in the range (E_B, E_m) can be characterised as follows. There exists a hyperbolic set Λ of measure zero consisting of localised trajectories which have an infinite number of intersections with the Poincaré surface, both forward and backward in time. The rest of the energy surface consists of orbits which reach out to infinity as time goes to $+\infty$ and/or $-\infty$, and have only a finite number of intersections with the Poincaré plane in forward and/or backward time. For points of Λ we found a globally exact symbolic dynamics which turned out to be binary; therefore the Poincaré mapping of our system is a perfect realisation of a Smale horseshoe map. To any infinite binary sequence there corresponds exactly one localised trajectory of the symmetry reduced system, and vice versa, each localised trajectory is characterised uniquely by an infinite binary sequence. In particular, this complete symbolic dynamics provides full knowledge of all periodic orbits because periodic orbits are in one–to–one correspondence with periodic symbolic sequences. It is remarkable that this picture of a perfect horseshoe holds true over the relatively large energy interval $(E_B, E_m) \approx (0.485, 1.005)$. No bifurcations of localised orbits occur in this interval.

When E falls towards $E_B \approx 0.485$, the point R_2 of figure 3 is $(r, p_r) = (0, 0)$, and for lower energies, the simple horseshoe picture ceases to be valid. The closure of the homoclinic points of P_γ no longer coincides with the closure of the homoclinic points of P_Γ. The two sets separate. The invariant set corresponding to P_γ disappears completely as $E \to E_s$. The invariant set corresponding to P_Γ loses its connection to the scattering orbits as $E < E_s$; it then forms the backbone of a region of bound chaos.

4. Symmetry classes of periodic orbits

The potential (1) possesses C_{3v} symmetry. Its symmetry elements are the three reflections at lines $\sigma_1, \sigma_2, \sigma_3$, and two rotations by $\pm 2\pi/3$ about the centre. In addition, our system possesses time reversal symmetry T. Let Φ_t denote the flow in phase space as given by the Hamiltonian $H = H(x, y, p_x, p_y)$:

$$\Phi_t : (x, y, p_x, p_y)_{\text{time}=0} \mapsto (x, y, p_x, p_y)_{\text{time}=t} \,. \tag{12}$$

Symmetry under time reversal

$$T : (x, y, p_x, p_y) \mapsto (x, y, -p_x, -p_y) \tag{13}$$

means that

$$\Phi_t = T \circ \Phi_{-t} \circ T. \tag{14}$$

From (13) and (14) it is obvious that T and $\Phi_t \circ T$ are involutions

$$T^2 = \mathrm{id} \qquad (\Phi_t \circ T)^2 = \mathrm{id}. \tag{15}$$

What are the invariant sets of T and $\Phi_t \circ T$, for a given t? From (13) we see that invariance of a phase space point under T requires $p_x = p_y = 0$. This defines a line in the energy surface $E =$ constant: the line of points at the boundary of the accessible potential range, where the kinetic energy is zero. The phase space points invariant under $\Phi_t \circ T$ are points $(\boldsymbol{x}, \boldsymbol{p})$ for which $\Phi_{-t/2}(\boldsymbol{x}, \boldsymbol{p})$ is invariant under T, i.e., they are the invariant set of T transported by the flow $\Phi_{t/2}$.

Before we translate these observations into the corresponding properties of our Poincaré map let us consider another such involutory symmetry of the system. Combination of reflection σ_1 with time reversal gives the symmetry operation $S := \sigma_1 \circ T$

$$S : (x, y, p_x, p_y) \mapsto (x, -y, -p_x, p_y) \tag{16}$$

for which an analogous relation to (15) holds:

$$S^2 = \mathrm{id} \qquad (\Phi_t \circ S)^2 = \mathrm{id}. \tag{17}$$

Again we can look for the invariant sets of S and $\Phi_t \circ S$ on a given energy surface. We find that the invariant line of S is the set of points $y = p_x = 0$, i.e. the orbits crossing the x axis perpendicularly. The invariant lines of $\Phi_t \circ S$ are obtained from them by the flow $\Phi_{t/2}$.

Two more such involutions are obtained from combination of σ_2 and σ_3 with T, but these will be identified with S by means of the C_{3v} rotations.

Let us now discuss what this implies for our Poincaré map $P : \mathcal{P} \to \mathcal{P}$. Given an energy E, the surface of section *before* symmetry reduction, defined by $y = 0, x > 0$, consists of two sheets: one with $p_y > 0$, the other with $p_y < 0$. The operation T leads back and forth between the two sheets. The operation S, on the other hand, preserves p_y and thus stays on the same sheet. The sheets happen to contain the part $x > 0$ of the invariant lines of S.

After symmetry reduction, we identify a phase space point (x, y, p_x, p_y) with its image under σ_1, $(x, -y, p_x, -p_y)$, and therefore also the operations T and $S = \sigma_1 \circ T$. Denoting henceforth the restriction of these operations to the Poincaré surface by R

$$R : (r, p_r) \mapsto (r, -p_r) \tag{18}$$

the two equations (15) and (17) combine into

$$R^2 = \mathrm{id} \qquad (P \circ R)^2 = \mathrm{id}. \tag{19}$$

The invariant set of R is now the line

$$\mathcal{R}_0 = \{(r, p_r) | p_r = 0\}. \tag{20}$$

The invariant set of $P \circ R$ consists of two parts $\mathcal{R}_1^\tau$ and $\mathcal{R}_1^\sigma$ (see figure 4). The line $\mathcal{R}_1^\tau$ is the invariant set of T transported by the flow until it first crosses the Poincaré surface, and $\mathcal{R}_1^\sigma$ is the part $x < 0$ of the invariant set of S transported into $\mathcal{P}$.

Given the elementary lines $\mathcal{R}_0$, $\mathcal{R}_1^\tau$, $\mathcal{R}_1^\sigma$, we may subject them to forward and backward iteration under P:

$$\begin{aligned} \mathcal{R}_{2n} &:= P^n \mathcal{R}_0 \\ \mathcal{R}_{2n+1}^\tau &:= P^n \mathcal{R}_1^\tau \\ \mathcal{R}_{2n+1}^\sigma &:= P^n \mathcal{R}_1^\sigma \end{aligned} \tag{21}$$

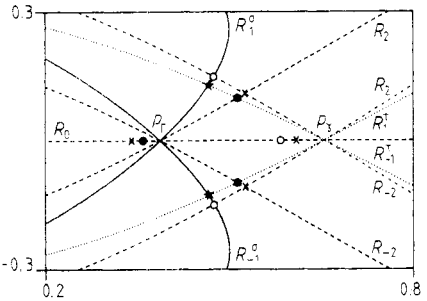

Figure 4. The elementary symmetry lines and some of their images under P in the r/p_r plane. Some periodic orbits with low periods are marked.

($n \in \mathbb{Z}$). The two sets $\mathcal{R}_{2n+1}^\tau$ and $\mathcal{R}_{2n+1}^\sigma$ will together be denoted by $\mathcal{R}_{2n+1}$. The following facts are then true (see e.g. [1]):

(i) $\mathcal{R}_m$ is the invariant set of $P^m \circ R (m \in \mathbb{Z})$.

(ii) The intersections of $\mathcal{R}_m$ and $\mathcal{R}_n$ are points of period $|m-n|$.

Iterating the lines $\mathcal{R}_0$, $\mathcal{R}_1^\tau$, $\mathcal{R}_1^\sigma$, we thus obtain periodic orbits by looking for intersections of these lines and their iterates. Figure 4 gives a few examples. The two fixed points are identified as

$$P_\gamma = \mathcal{R}_0 \cap \mathcal{R}_1^\tau \qquad P_\Gamma = \mathcal{R}_0 \cap \mathcal{R}_1^\sigma. \tag{22}$$

There is an orbit of period 2 given as

$$\mathcal{R}_1^\tau \cap \mathcal{R}_{-1}^\sigma \mapsto \mathcal{R}_{-1}^\tau \cap \mathcal{R}_1^\sigma \mapsto \mathcal{R}_1^\tau \cap \mathcal{R}_{-1}^\sigma. \tag{23}$$

This orbit is marked by a star; the corresponding trajectory in position space is shown in figure 5(b). Two period 3 orbits are shown, represented by the points

$$\mathcal{R}_1^\tau \cap \mathcal{R}_{-2} \qquad \text{and} \qquad \mathcal{R}_1^\sigma \cap \mathcal{R}_{-2}. \tag{24}$$

The first is marked by full circles; its trajectory is shown in figure 5(c). The second is marked by open circles; its trajectory is shown in figure 5(i). The orbit of period 4 given by

$$\mathcal{R}_2 \cap \mathcal{R}_{-2} \tag{25}$$

is marked by crosses; its trajectory is shown in figure 5(m).

The interesting question is how the periodic orbits so determined compare to the symbolic identification as introduced in section 3. The connection is quite simple. It is based on the following facts.

(i) The line $\mathcal{R}_0$ is the set of all points whose symbolic signature (finite or infinite) is symmetric with respect to the dot:

$$\mathcal{R}_0 \simeq \{\ldots a_n \ldots a_2 a_1 . a_1 a_2 \ldots a_n \ldots | a_j \in \{0,1\}\}. \tag{26}$$

The reason is of course the σ_i-symmetry of the system; an orbit crossing a line σ_i orthogonally produces the same sequence of symbols in forward and backward direction.

(ii) The line $\mathcal{R}_1^\tau$ is the set of all points whose signature (finite or infinite) is symmetric with respect to 0.:

$$\mathcal{R}_1^\tau \simeq \{\ldots a_n \ldots a_2 a_1 0.a_1 a_2 \ldots a_n \ldots | a_j \in \{0,1\}\}. \tag{27}$$

The reason is that the points of $\mathcal{R}_1^\tau$ have been transported into $\mathcal{P}$ from an encounter with the boundary of the accessible potential range. Their orbits in configuration space, viewed from that encounter, are identical in forward and backward time; the piece containing the reflection at the potential border must be of type $\frac{1}{2}\gamma$.

(iii) The line $\mathcal{R}_1^\sigma$ is the set of all points whose signature (finite or infinite) is symmetric with respect to 1.:

$$\mathcal{R}_1^\sigma \simeq \{\ldots a_n \ldots a_2 a_1 1.a_1 a_2 \ldots a_n \ldots | a_j \in \{0,1\}\}. \tag{28}$$

The reason is that the points of $\mathcal{R}_1^\sigma$ have been transported into $\mathcal{P}$ from a perpendicular crossing of the extensions of the σ_i lines. Their orbits in configuration space, viewed from that crossing, are symmetric with respect to reflections at σ_i; the piece containing this crossing must by of type $\frac{1}{3}\Gamma$.

Iterates of the basic symmetry lines $\mathcal{R}_0$, $\mathcal{R}_1^\tau$, $\mathcal{R}_1^\sigma$ simply have the points of symmetry in their sequences right or left shifted. It is now obvious that points from intersections of two such lines correspond to periodic orbits: they have two points of symmetry in their sequence, so the sequence must be repetetive. In the following we shall represent orbits of period p by their basic repetetive blocks of p symbols, $a_1 a_2 \ldots a_p$.

We are now in a position to give a complete survey on the periodic orbits with respect to their symmetry properties. Let us introduce the symbols _, $\overline{0}$, $\overline{1}$ to denote spaces, zeroes, and ones with respect to which a 0/1-sequence is symmetric. There are seven classes of periodic orbits.

C^{00}: Intersections of type $\mathcal{R}_0 \cap \mathcal{R}_{2n}$ are periodic orbits whose sequence contains a _ at two positions. Example: 0_01_1 (see figure 5(m)).

$C^{0\tau}$: Intersections of type $\mathcal{R}_0 \cap \mathcal{R}_{2n+1}^\tau$ are periodic orbits whose sequence contains a _ and a $\overline{0}$. Examples: $\overline{0}\_, \overline{0}1\_1, \overline{0}11\_11, 0\_01\overline{0}1$ (see figure 5(a, c, e, n)).

$C^{0\sigma}$ Intersections of type $\mathcal{R}_0 \cap \mathcal{R}_{2n+1}^\sigma$ are periodic orbits whose sequence contains a _ and a $\overline{1}$. Examples: $\overline{1}\_, 0\_0\overline{1}, 00\_00\overline{1}$ (see figure 5(g, i, k)).

$C^{\tau\tau}$ Intersections of type $\mathcal{R}_1^\tau \cap \mathcal{R}_{2n+1}^\tau$ are periodic orbits whose sequence contains two symbols $\overline{0}$. Example: $0\overline{0}01\overline{0}1$ (see figure 5(o)).

$C^{\sigma\sigma}$ Intersections of type $\mathcal{R}_1^\sigma \cap \mathcal{R}_{2n+1}^\sigma$ are periodic orbits whose sequence contains two symbols $\overline{1}$. Example: $0\overline{1}01\overline{1}1$ (figure 5(p) shows one third of this orbit).

$C^{\tau\sigma}$ Intersections of type $\mathcal{R}_1^\tau \cap \mathcal{R}_{2n+1}^\sigma$ are periodic orbits whose sequence contains a $\overline{0}$and a $\overline{1}$. Examples: $\overline{0}\overline{1}, \overline{0}1\overline{1}1, \overline{0}11\overline{1}11, 0\overline{0}0\overline{1}, 00\overline{0}00\overline{1}$ (see figure 5(b, d, f, j, l)).

C^{--} The rest of the periodic orbits cannot be obtained from intersection of the symmetry lines. Examples: figure 5(q) shows one half of the orbit 001011, and figure 5(r) shows one third of 0001101.

Let us now explore the symmetry properties of the various types of periodic orbits, and at the same time the multiplicities of the corresponding points in the symmetry reduced Poincaré section. As C_{3v} has six elements, a given point of our Poincaré surface $\mathcal{P}$ represents altogether six different points in the full phase space. The corresponding time reversed points are obtained by reflection R. Remember from above (see (18)) that R is the symmetry reduction of both T and S. Therefore, if a symmetry reduced

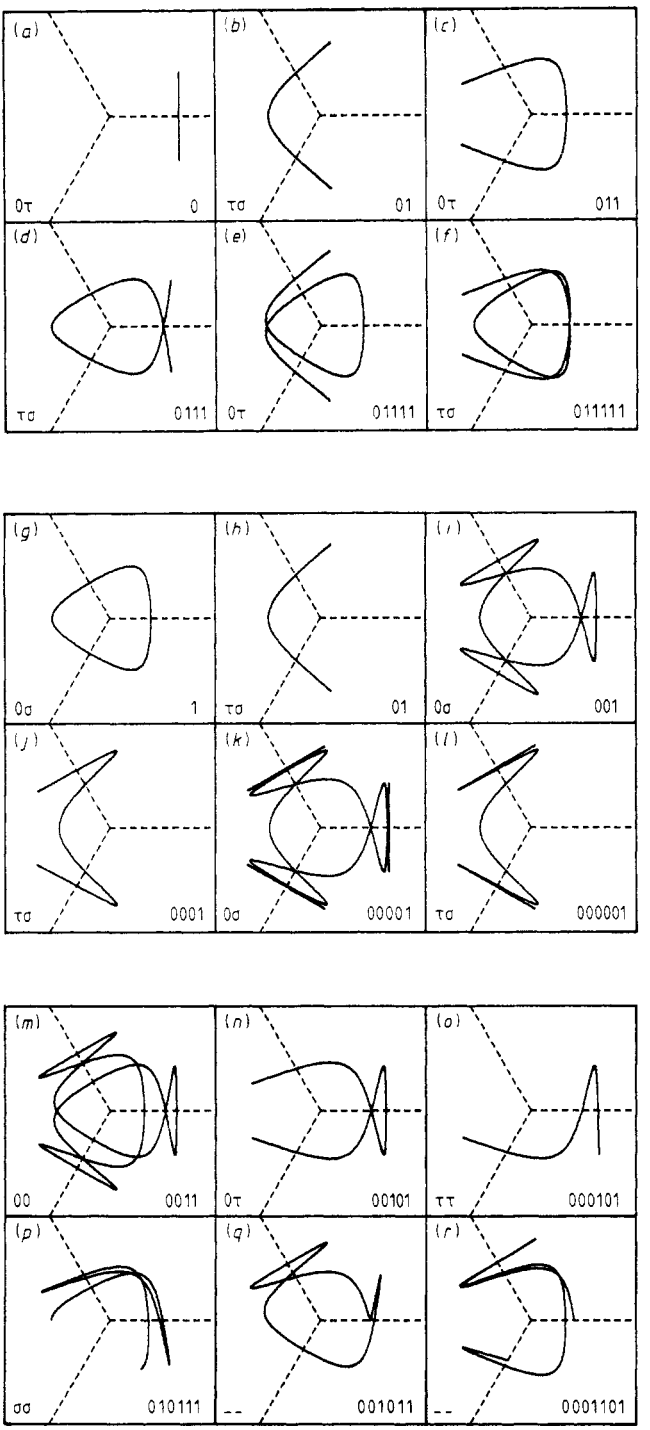

Figure 5. 18 examples of periodic orbits of low periods in position space. To each orbit we give the symmetry class in the lower left corner, and the basic block of the symbolic signature in the lower right corner.

periodic orbit shows symmetry with respect to the axis $r = 0$, its counterpart in full phase space may be symmetric under T, or S, or both. If it is not symmetric under T, then each corresponding non-reduced orbit has a reflection symmetric trace which can be traversed in two orientations (classes $C^{00}, C^{0\sigma}, C^{\sigma\sigma}$). If it is not symmetric under S, then each corresponding non-reduced orbit is traversed in both directions but has no reflection symmetry (class $C^{\tau\tau}$).

To discuss whether or not a periodic orbit is invariant under rotations D, we introduce one more detail in the notation. Depending on the orientation of a $\frac{1}{3}\Gamma$ piece in a given orbit, we replace the symbols 1 in the 0/1 sequences by + (for positive), or by − (for negative rotation). The sequence 0011, e.g., can then appear as 00++ or as 00−− = T(00++). The sequence 00101101 can have the two forms 00+0−−0+ and (its image under T) 00−0++0−. Note that each intervening 0, i.e. each orbit segment of type $\frac{1}{2}\gamma$, enforces a change in orientation of the $\frac{1}{3}\Gamma$ piece (therefore the ± notation is strictly speaking unnecessary, but it helps in the following; the signature remains binary in nature). Adding the signs in the case ofthe orbit 0011 , we get ±2, whereas in the case of 00101101 we get the sum 0. This indicates that in the first case, when we start on a given σ_i line, the sequence 0011 will lead us to another σ_i line, whereas in the second case the sequence 00101101 leads us back to the starting line. As a result, the orbit 00101101, in the non-reduced phase space, is closed after one scan through the sequence of eight symbols, and it comes in three copies, related by rotations D. The orbit 0011, on the other hand, needs three scans before it is closed in the non-reduced phase space; accordingly it has twelve intersections with lines σ_i, but the orbit itself is invariant under rotations D.

Let us call the sum of the orientation signs of a periodic orbit its Γ sum. If the Γ sum is 0 mod 3, the orbit has no rotational symmetry, and there are three different copies related by D (these orbits may be said to belong to the representation E of C_{3v}). If the Γ sum is ±1 mod 3, the orbit itself shows rotational symmetry.

This is a list of the symmetry properties of the various classes of orbits.

(1) Class C^{00} orbits have an even number of 0/1 symbols. They come in two types, depending on their Γ sum.

(*a*) Orbits with zero Γ sum modulo 3 (like 00101101) possess only S symmetry but no D nor T symmetry. Each symmetry reduced orbit stands for six different non-reduced orbits.

(*b*) Orbits with non-zero Γ sum modulo 3 (like 0011) possess S and D symmetry but no T symmetry. Each symmetry reduced orbit stands for two different non-reduced orbits.

(2) Class $C^{0\tau}$ orbits have an odd number of 0/1 symbols. They possess S and T symmetry but no D symmetry (after two scans through the sequence the non-reduced orbit is always back at the starting σ line). Each symmetry reduced orbit stands for three different non-reduced orbits.

(3) Class $C^{0\sigma}$ orbits have an odd number of 0/1 symbols. They come in two types, depending on their Γ sum.

(*a*) Orbits with zero Γ sum modulo 3 (like 00111) possess only S symmetry but no D nor T symmetry. Each symmetry reduced orbit stands for six different non-reduced orbits.

(*b*) Orbits with non-zero Γ sum modulo 3 (like 1 or 001) possess S and D symmetry but no T symmetry. Each symmetry reduced orbit stands for two different non-reduced orbits.

(4) Class $C^{\tau\tau}$ orbits have an even number or 0/1 symbols. They possess only T symmetry but neither S nor D symmetry. Each symmetry reduced orbit stands for six different non-reduced orbits.

(5) Class $C^{\sigma\sigma}$ orbits have an odd number of 0/1 symbols. They come in two types, depending on their Γ sum.

(*a*) Orbits with zero Γ sum modulo 3 (like 0101111111) possess only S symmetry but no D nor T symmetry. Each symmetry reduced orbit stands for six different non-reduced orbits.

(*b*) Orbits with non-zero Γ sum modulo 3 (like 010111) possess S and D symmetry but no T symmetry. Each symmetry reduced orbit stands for two different non-reduced orbits.

(6) Class $C^{\tau\sigma}$ orbits have an even number of 0/1 symbols. They possess S and T symmetry but no D symmetry. Each symmetry reduced orbit stands for three different non-reduced orbits.

(7) Class C^{--} orbits must have at least period 6 (in the symmetry reduced Poincaré surface). Their proportion among all periodic orbits grows as the period increases. As to their symmetry properties, little can be said. The example 001011 (see figure 5(*q*)) has σ symmetry but neither T nor D symmetry; it stands for six different non-reduced orbits of period 12. The example of figure 5(*r*), 0001101 has D symmetry but neither T nor σ symmetry; it stands for four different non-reduced orbits of period 21. We do not know whether there are periodic orbits with no symmetry whatsoever.

Our characterisation of periodic orbits has come from two seemingly different sides. In section 3 we used the invariant manifolds to define the invariant set Λ with its symbolic dynamics. In this section we used symmetry lines to identify periodic orbits, and have not said anything about invariant manifolds and homoclinic or heteroclinic orbits. Yet there is an intimate connection. The higher iterates of the symmetry lines approach the invariant manifolds ever more closely, and the periodic orbits of increasing periods approximate homoclinic and heteroclinic points. The closure of the set of intersections of the lines $\mathcal{R}_n$ is again the invariant set Λ. We do not want to discuss this well known fact in more detail except to point out that the combination of symmetry lines with the invariant manifolds suggests the definition of families of periodic orbits, with periods increasing towards ∞, each family converging towards a homoclinic orbit. Consider, e.g., the sequence of orbits 1, 01, 001, 0001, ... shown in figure 5(*g–l*). It converges towards the homoclinic orbit ...00001.0000..., i.e. the solitary crossover from one infinite sequence of saddle oscillations γ to another. This orbit contains the points Q_1, Q_2, Q_3, Q_4 of figure 3. We can view it as the limit of the sequence of orbits $\mathcal{R}^{\sigma}_{-1} \cap \mathcal{R}_m (m = 0, 1, 2, \ldots)$ which line up along the line $\mathcal{R}^{\sigma}_{-1}$(see figure 4). Their symmetry class alternates between $C^{0\sigma}$ and $C^{\tau\sigma}$ depending on $\mathcal{R}_m$ being $\mathcal{R}_{2n}$ for even m or $\mathcal{R}^{\tau}_{2n+1}$ for odd m.

Another family of a similar kind is the sequence of orbits 0, 01, 011, 0111, ... shown in figure 5(*a–f*). It converges towards the homoclinic orbit ...11110.1111..., i.e. the once in a lifetime return from one infinite sequence of rotations Γ to the reversed sequence. This orbit is not shown in figure 3 because we did not draw the invariant manifolds of the point P_Γ; they are, of course, contained in the closure of the invariant manifolds of P_γ. This family can be viewed as the sequence of intersections $\mathcal{R}^{\tau}_{-1} \cap \mathcal{R}_m (m = 0, 1, 2, \ldots)$ along the line $\mathcal{R}^{\tau}_{-1}$. Their symmetry class alternates between $C^{0\tau}$ and $C^{\tau\sigma}$ depending on whether $\mathcal{R}_m$ is $\mathcal{R}_{2n}$ or $\mathcal{R}^{\sigma}_{2n+1}$. Such families of

orbits tend to behave in a concerted way when a system parameter is varied (e.g. the energy).

5. Scaling properties

The simplicity of the horseshoe structure in figure 3 suggests, in a first approximation, to assume affinity of the Poincaré map P on Λ, and to characterise it completely by the eigenvalues of P at the fixed points P_γ and P_Γ. The hierarchy of scaling factors is thereby assumed to be self-similar. This picture is qualitatively correct in the energy range $(E_B, E_m) = (0.485, 1.005)$. A quantitative test will be made for the case $E = 0.6$, by comparison with a full computation of the fractal characteristics. For energies smaller than E_B, the affine approximation can still be computed and will be shown in the following pictures; its validity, however, is questionable.

Our analysis of the metric properties of the fractal structures will be based on the thermodynamic formalism of multifractals. A good introductory review of this matter has been given recently by Tél [8]. Our aim here is only to demonstrate that the invariant set Λ is adequately understood as a two-scale fractal, and that its various 'dimensions' have a simple energy dependence. We recall that the thermodynamic formalism focuses on the purely *geometric* properties of fractals, i.e. on the distribution of length scales among its various parts, while the more traditional multifractal analysis [9, 10] aims at characterising *measures* that the fractals carry.

Let κ and $1/\kappa$ ($\kappa > 1$) be the eigenvalues of P at P_γ, ν and $1/\nu$ ($\nu < -1$) the eigenvalues at P_Γ (P_Γ is inverse hyperbolic). (In the non-reduced Poincaré map of [2] the eigenvalues of γ and Γ were denoted by μ and λ; the connection is $\kappa = \mu^{1/2}, \nu = \lambda^{1/3}$.) Figure 6 shows the eigenvalues as functions of the energy, in the energy range $E \in (E_s, E_m)$. For $E \to E_m$ they tend to infinity, $\kappa \to \infty, \nu \to -\infty$. As $E \to E_s$, the eigenvalue κ at P_γ tends to $6.9\ldots$ which can be computed analytically (see [2]); $\nu = -1.3\ldots$ at $E = E_s$. The orbit P_γ vanishes at $E = E_s$ whereas P_Γ continues to exist in an interval (E_o, E_s), turning elliptic for $E < E_c$ with E_c somewhat smaller than E_s.

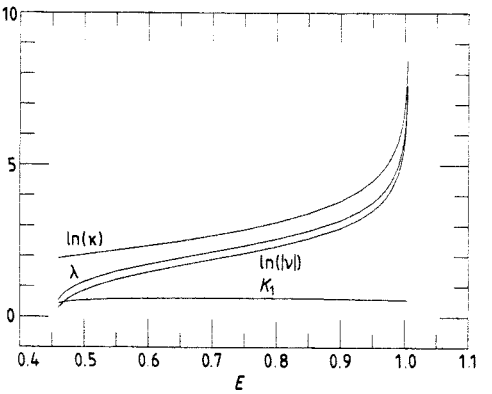

Figure 6. The logarithms of the eigenvalues κ and $|\nu|$ of the fixed points P_γ and P_Γ in the symmtery reduced Poincaré map P, as functions of the energy. Also shown are the Lyapunov number as given by (37), and the Kolmogorov entropy according to (43).

The invariant set Λ is the direct product of two Cantor sets Λ^s and Λ^u where Λ^s is the intersection of Λ with the segment $P_\gamma Q_3$ of the stable manifold of P_γ (see figure 3), and $\Lambda^u = R(\Lambda^s)$. The set Λ^s consists of two disjoint parts which are contractions of the total, by factors $r_1 = 1/\kappa$ and $r_2 = -1/\nu$ respectively. Such fractals have been considered extensively in the literature, see e.g. [10, 11], and [8] for a review. They are geometric multifractals whose length scales on the nth level are $r_1^m r_2^{n-m}$ where m is the number of 0's, and $n - m$ the number of 1's in the binary sequence of the piece under consideration. The statistical properties of Λ can be derived from the partition function

$$\sum (r_1^m\, r_2^{n-m})^\beta =: \mathrm{e}^{-\beta F(\beta) n} \tag{29}$$

where the sum is taken over all sequences of length n ($n \gg 1$). Using Stirling's rule in the evaluation of binomial coefficients we find the $F(\beta)$ function to be

$$\beta F(\beta) = -\log(r_1^\beta + r_2^\beta). \tag{30}$$

According to the thermodynamic formalism the corresponding 'energies' U and 'entropies' $S = S(U)$ can be derived via

$$U = \frac{\partial}{\partial \beta} \beta F \qquad S = \beta(U - F). \tag{31}$$

The quantity U measures how rapidly the length scales decrease with increasing n: its value for a piece with a given symbolic sequence is

$$U = -\frac{1}{n} \log(r_1^m\, r_2^{n-m}). \tag{32}$$

$S(U)$ characterises the number $W(n, U)$ of pieces of the same size, with sequences of length n, and belonging to a given value of U:

$$W(n, U) = \mathrm{e}^{S(U) n}. \tag{33}$$

Using β as a parameter, it is straightforward to plot the $S(U)$ spectra. Figure 7 shows $\beta F(\beta)$ and $S(U)$ for a number of energies E.

Assuming equidistribution of points in phase space, we can deduce from this purely geometric description of our fractals the characterisation of the measure that they carry. As has been shown in [8], the Hölder exponents α and the spectrum of fractal dimensions $f(\alpha)$ of this measure are given by

$$\alpha = 1 - \frac{F(1)}{U} \qquad f(\alpha) = \frac{S}{U}. \tag{34}$$

Similarly, the 'order q generalised dimensions' $D(q)$ are related to the 'thermodynamic' quantities via

$$q = \frac{\beta F}{F(1)} \qquad D_q = \frac{q - \beta}{q - 1}. \tag{35}$$

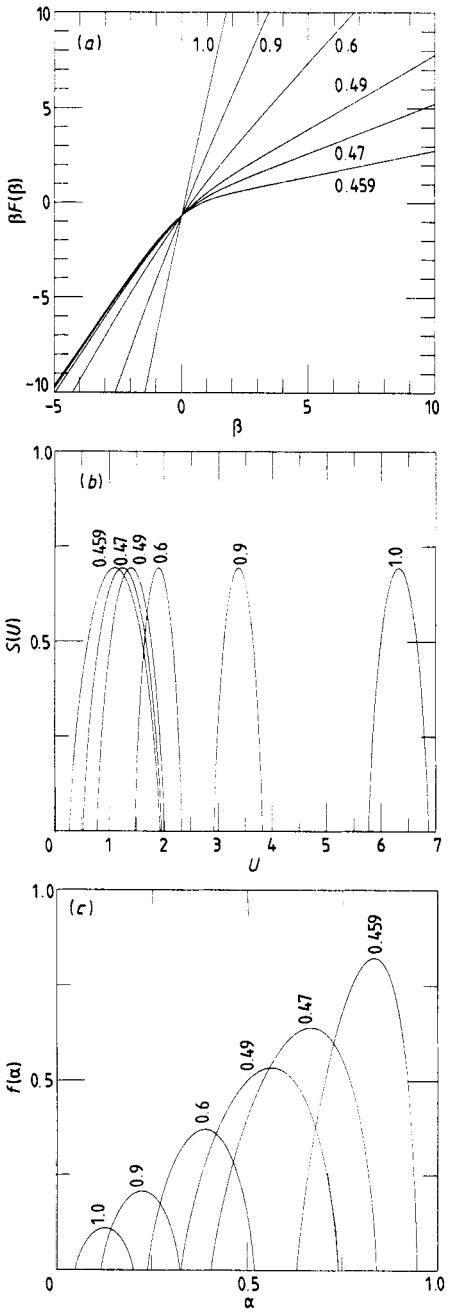

Figure 7. (a) $\beta F(\beta)$ against β for six different energies between $E = 0.459$ and $E = 1.0$. The horseshoe picture on which (30) is based holds for $E > E_B \approx 0.485$. (b) $S(U)$ against U for the same energies; the range of possible U values is $(\log|\nu|, \log\kappa)$. (c) $f(\alpha)$ against α for the same energies.

We can also give the generalised entropies K_q

$$K_q = \frac{q(F(\beta(q)) - F(1))}{q-1} \tag{36}$$

and the Lyapunov exponent λ

$$\lambda = U(\beta = 1) = -\frac{r_1 \log r_1 + r_2 \log r_2}{r_1 + r_2}. \tag{37}$$

All these quantities are contained in the 'free energy' $F(\beta)$.

Let us discuss a few special characteristics of Λ. Its fractal dimension D_0 is the value of β for which $F(\beta) = 0$; it is also the maximum value of $f(\alpha)$. As figure 8 shows, it decreases systematically as the energy E increases. According to [12] this decrease should follow the law

$$D_0 \sim -1/\log(E_m - E) \tag{38}$$

as $E \to E_m$. This non-analytic behaviour is an immediate consequence of

$$r_1^{D_0} + r_2^{D_0} = 1 \tag{39}$$

if $r_1 \sim (E_m - E)^x$ and $r_2/r_1 \to$ constant as $E \to E_m$, where x is any power.

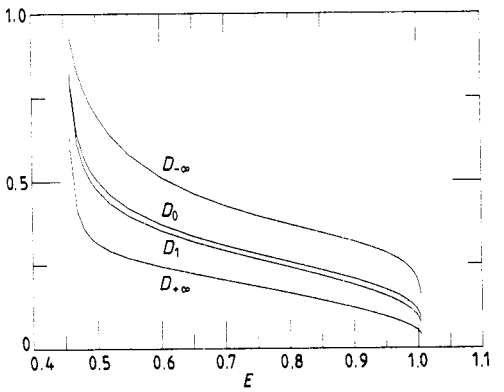

Figure 8. The dependence of fractal dimensions on the energy in the range $E_B \leq E \leq E_m$. D_0 is the fractal dimension, D_1 the information dimension; all other D_q are between D_∞ and $D_{-\infty}$.

The information dimension D_1 can be derived analytically from (35):

$$D_1 = \frac{(r_1 + r_2)\log(r_1 + r_2) - r_1 \log r_1 - r_2 \log r_2}{r_1 \log r_2 + r_2 \log r_1}. \tag{40}$$

It is also shown in figure 8, together with the minimum and maximum values $D_{q\to\infty}$ and $D_{q\to-\infty}$. These values are obtained from the limits $\beta \to \pm\infty$ of $\beta F(\beta)$. We have

$$F(\beta), U \to \begin{cases} -\log r_1 = \log \kappa & (\beta \to -\infty) \\ -\log r_2 = \log|\nu| & (\beta \to \infty) \end{cases} \tag{41}$$

and consequently

$$D_q, \alpha \to \begin{cases} 1 - F(1)/\log \kappa & (\beta \to -\infty) \\ 1 - F(1)/\log|\nu| & (\beta \to \infty) \end{cases} \tag{42}$$

This shows that the limiting values of U are given by the eigenvalues κ and ν only whereas the limiting values of D_q and α also involves $F(1)$ which can be interpreted as the *escape rate* [13].

The topological entropy $K_{q=0} = -\beta F|_{\beta=0} = \log 2$ reflects the binary coding of the scattering dynamics; for $q = 1$ we obtain the Kolmogorov entropy

$$K_{q=1} = \lambda - F(1) = \frac{(r_1 + r_2)\log(r_1 + r_2) - r_1 \log r_1 - r_2 \log r_2}{r_1 + r_2} \tag{43}$$

where λ is the Lyapunov exponent. K_1 and λ are plotted together with the eigenvalues in figure 6.

In order to test the validity of the approximation based on the two eigenvalues κ and ν, for $E = 0.6$, we have computed some thermodynamic quantities from the lengths of the intervals that are to be cut out in the recursive construction of Λ^s. These intervals were determined with sufficient precision to the eighth generation, and from their lengths $\ell_i^{(n)}$ in generation n, $i = 1 \ldots 2^n$, we determined $F(\beta)$ according to the recipe given in [13]

$$\sum_{i=1}^{2^n} \ell_i^{(n)\beta} \sim \mathrm{e}^{-\beta F(\beta) n}. \tag{44}$$

Using β as a parameter, we calculated the function $S = S(U)$. The result is shown in figure 9 where a comparison with the eigenvalue approximation is made. The agreement is quite satisfactory. The points calculated by (44) span a slightly larger range of U values because numerical errors in the determination of the lengths $\ell_i^{(n)}$ tend to increase the interval of scaling factors.

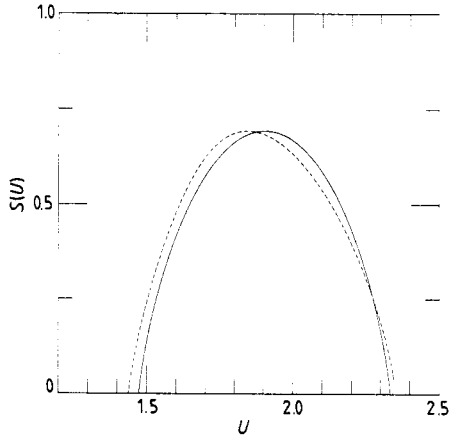

Figure 9. Comparison of $S = S(U)$ as given by the intervals of lengths $\ell_i^{(8)}$, $i = 1 \ldots 256$, (broken curve, computed by means of (44)), with the eigenvalue approximation (full curve, computed with (31)). The energy is $E = 0.6$.

6. Concluding remarks

The method of iterated symmetry lines is a powerful tool to obtain sets of periodic orbits in a Hamiltonian system. The periodic orbits are of interest because they

organise the system's dynamics: as elliptic centres of order or as hyperbolic centres of chaos. Recently it has become evident that they are particularly important in connection with the semiclassical quantisation of classically chaotic systems [14, 15, 16]. It is therefore important to know what proportion of the totality of periodic orbits can be determined by the method of symmetry line iteration.

We have analysed this question for the example of a scattering system where a complete survey on the periodic orbits exists. This survey is provided by the fact that the Poincaré map of this system contains a perfect horseshoe map with its corresponding symbolic dynamics. This allows us to investigate systematically which periodic orbits are missed by the symmetry line method. We approach the invariant set Λ of the horseshoe map using the symmetry line technique and characterise the subset of periodic orbits that can be derived in this way. These orbits can be grouped into classes each of which reflects some of the system's symmetry properties; these symmetries can also be expressed in terms of the binary symbolic sequences that correspond to the orbits. It turns out that in the case studied, all periodic orbits with periods up to 5 (in a symmetry reduced Poincaré surface of section) can be obtained as intersections of the symmetry lines. The first orbits that cannot be obtained in this way have period 6. Their proportion increases with increasing period and becomes dominant as the period tends to infinity. Luckily, the more conspicuous properties of the system's chaotic dynamics tend to be related to the periodic orbits of low periods [17], but as the example of the Trojan asteroids in celestial mechanics shows, there are Hamiltonian systems which exhibit notable exceptions from this rule.

The simplicity of the horseshoe map in the case under study has allowed us to give a comprehensive characterisation of the multifractal properties of the invariant set Λ. Using the assumption of affine dynamics on the set Λ we were able to compute the energy depence of its various fractal dimensions on the basis of the thermodynamic formalism as presented by Tél [8]. Comparison with direct computation shows that this simplifying assumption is well justified.

Acknowledgments

We are indebted to Tamás Tél for illuminating discussions on the thermodynamic formalism for multifractals.

References

[1] Richter P H, Scholz H-J and Wittek A 1989 A breathing chaos *Nonlinearity* **3** 45–67
[2] Jung C and Scholz H-J 1987 Cantor set structures in the singularities of classical potential scattering *J. Phys. A: Math. Gen.* **20** 3607–17
[3] Jung C and Pott S 1989 Classical cross section for chaotic potential scattering *J. Phys. A: Math. Gen.* **22** 2925–38
[4] Troll G and Smilansky U 1989 A simple model for chaotic scattering I. Classical theory *Physica* **35D** 34–64
[5] Eckhardt B 1987 Fractal properties of scattering singularities *J. Phys. A: Math. Gen.* **20** 5971–9
[6] Gaspard P and Rice S A 1989 Scattering from a classically chaotic repellor *J. Chem. Phys.* **90** 2225-41
[7] Jung C and Scholz H-J 1988 Chaotic scattering off the magnetic dipole *J. Phys. A: Math. Gen.* **21** 2301–11
[8] Tél T 1988 Fractals, multifractals and thermodynamics *Z. Naturforsch.* **43a** 1154–74

[9] Mandelbrot B B 1974 Intermittent Turbulence in Self Similar Cascades; Divergence of High Moments and Dimension of the Carrier *J. Fluid Mech.* **62** 331

[10] Halsey T, Mogens H J, Kadanoff L P, Procaccia I and Shraiman B I 1986 Fractal measures and their singularities: The characterisation of strange sets *Phys. Rev.* A **33** 1141–51

[11] Tél T 1989 On the organisation of transient chaos—application to irregular scattering *J. Phys. A: Math. Gen.* **22** L691–97

[12] Bleher S, Ott E and Grebogi C 1989 Routes to chaotic scattering *Phys. Rev. Lett.* **63** 919–22

[13] Kovacs Z and Tél T 1990 The thermodynamics of irregular scattering *Phys. Rev. Lett.* **64** 1617–20

[14] Gutzwiller M C 1971 Periodic orbits and classical quantisation conditions *J. Math. Phys.* **12** 343–58

[15] Wintgen D and Friedrich H 1987 Correspondence of unstable periodic orbits and quasi-Landau modulations *Phys. Rev.* A **36** 131–42

[16] Cvitanović P and Eckhardt B 1989 On periodic orbit quantisation of chaotic systems *Phys. Rev. Lett.* **63** 823–6

[17] Cvitanović P 1988 Invariant measurement of strange sets in terms of cycles *Phys. Rev. Lett.* **61** 2729–32